5. K. T. Schomacker, O. Bangcharoenpaurpong, P. M. Champion, *J. Chem. Phys.* **80**, 4701 (1997).
6. S. Franzen, B. Bohn, C. Poyart, J. L. Martin, *Biochemistry* **34**, 1224 (1995).
7. J. L. Martin *et al*., *Proc. Natl. Acad. Sci. U.S.A.* **80**, 173 (1983).
8. J. W. Petrich, J. L. Martin, D. Houde, C. Poyart, A. Orszag, *Biochemistry* **26**, 7914 (1987).
9. P. A. Anfinrud, C. Han, R. M. Hochstrasser, *Proc. Natl. Acad. Sci. U.S.A.* **86**, 8387 (1989).
10. Seed pulses from a mode-locked Ti:sapphire oscillator (Tsunami 3950, Spectra-Physics) were put into a regenerative amplifier (Spitfire, Positive Light) pumped by an Nd:yttrium-lithium-fluoride (Nd:YLF) laser operated at 1 kHz. The amplified output was composed of 2.5-ps pulses with energies of ~0.6 mJ at 784 nm. The pump pulse at 540 nm was generated with a homemade optical parametric generator (OPG) and amplifier (OPA), which were pumped with the second harmonic of the 784-nm output. (For details about the OPG-OPA system, see Y. Uesugi, Y. Mizutani, T. Kitagawa, *Rev. Sci. Instrum.*, in press.) The probe pulse at 435 nm was generated as the first Stokes stimulated Raman scattering from compressed (50 kg/cm$^2$) methane gas excited by the second harmonic of the 784-nm output. The energy and bandwidth of the OPG-OPA output were 30 μJ and ~3 nm, respectively, and the pulses were used for the pump beam in the present TR$^3$ measurements after they were attenuated to 10 μJ with a Cr-coated quartz neutral density filter. The energy and bandwidth of the stimulated Raman scattering were 1.0 to 1.5 μJ and 14 cm$^{-1}$, respectively. The pump and probe beams were colinearly combined with a dichroic mirror. The polarization of the pump beam was rotated by 55° relative to that of the probe beam to minimize the effects of molecular rotations on the observed kinetics. Both beams were always monitored with photodiodes and found to be stable within ±10%. Raman scattering was collected and focused onto the entrance slit of a single-stage imaging spectrograph (500IM-CM, Chromex) by using two doublet achromats. A dichroic filter was placed between the lenses to reject the scattered pump beam. A holographic notch filter (Kaiser Optical Systems) was used to reject the unshifted scattering. A polarization scrambler was placed at the entrance slit to remove the effects of polarization from the spectrograph throughput. The spectrograph was equipped with a blazed-holographic grating (2400 grooves per millimeter), which enables us to measure a spectrum as wide as ~900 cm$^{-1}$ in the Soret region with a spectral slit width of 10 cm$^{-1}$. The dispersed light was detected with a liquid nitrogen–cooled charge-coupled device detector (CCD-1100PB, Princeton Instruments). The 0 ps of delay time (uncertainty < 0.2 ps) was calibrated at the probe wavelength by using rhodamine 6G in methanol. The cross correlation width between the pump and probe pulses measured with a 1-mm β-barium borate crystal was 2.3 ps. Raman shifts were calibrated with indene. Peak positions of Raman bands are accurate within ±2 cm$^{-1}$.
11. Horse skeletal Mb (Sigma, type M630) was dissolved into deoxygenated buffer (50 mM tris-HCl, pH 8.0). The concentrated Mb solution was reduced by sodium dithionite, bubbled with CO gas, and subjected to gel filtration through a Sephadex G-25 column. The solution was diluted to 100 μM with deoxygenated and CO-saturated buffer (50 mM tris-HCl, pH 8.0) and put into an airtight quartz cuvette under a CO atmosphere. The sample solution in the cell was continuously stirred during the measurements to prevent multiple probing of the same portion of sample. Data accumulation time was 10 and 120 min for Stokes and anti-Stokes spectra, respectively. Sample integrity was confirmed with ultraviolet–visible absorption spectra after the TR$^3$ measurements.
12. M. Abe, T. Kitagawa, Y. Kyogoku, *J. Chem. Phys.* **69**, 4526 (1978).
13. S. Sato and T. Kitagawa, *Appl. Phys. B* **59**, 415 (1994); S. G. Kruglik, Y. Mizutani, T. Kitagawa, *Chem. Phys. Lett.* **266**, 283 (1997).
14. M. C. Simpson *et al*., *J. Am. Chem. Soc*. **119**, 5110 (1997).
15. The Boltzmann factor was represented in terms of the resonant Stokes and anti-Stokes scattering intensities in (*5*). With this expression we can, in principle, correct the differences between the Stokes and anti-Stokes scattering cross sections and determine an effective temperature of vibrational modes by analyzing their Raman excitation profiles.
16. Q. H. Gibson, J. S. Olson, R. E. McKinnie, R. J. Rohlfs, *J. Biol. Chem*. **261**, 10228 (1986).
17. P. Li and P. M. Champion [*Biophys. J*. **66**, 430 (1994)] used the two-boundary thermal transport model to analyze the thermal response to instantaneous heating of a chromophore embedded in a protein surrounded by water. The numerical solution of this model was well described by a double-exponential function in the short time limit, which "rolled over" into a diffusion-limited $t^{-3/2}$ decay (where $t$ is time) in the long time limit.
18. M. H. Keyes, M. Falley, R. Lumry, *J. Am. Chem. Soc.* **93**, 2035 (1971).
19. B. I. Greene, R. M. Hochstrasser, R. B. Weisman, W. A. Eaton, *Proc. Natl. Acad. Sci. U.S.A.* **75**, 5255 (1978).
20. E. R. Henry, W. A. Eaton, R. M. Hochstrasser, *ibid.* **83**, 8982 (1986).
21. T. Lian, B. Locke, Y. Kholodenko, R. M. Hochstrasser, *J. Phys. Chem.* **98**, 11648 (1994).
22. M. Lim, T. A. Jackson, P. A. Anfinrud, *ibid.* **100**, 12043 (1996)
23. J. R. Lingle, X. Xu, H. Zhu, S.-C. Yu, J. B. Hopkins, *ibid.* **95**, 9320 (1991).
24. Y.M. is a recipient of an Inoue Research Award for Young Scientists and gratefully acknowledges the Inoue Foundation for Science for partial support of this study. Supported by Grant-in-Aids for Scientific Research on Priority Areas (08249106) to T.K. from the Ministry of Education, Science, Sports, and Culture, Japan.

23 June 1997; accepted 2 September 1997

# DNA Solution of the Maximal Clique Problem

Qi Ouyang,* Peter D. Kaplan, Shumao Liu, Albert Libchaber

**The maximal clique problem has been solved by means of molecular biology techniques. A pool of DNA molecules corresponding to the total ensemble of six-vertex cliques was built, followed by a series of selection processes. The algorithm is highly parallel and has satisfactory fidelity. This work represents further evidence for the ability of DNA computing to solve NP-complete search problems.**

Computer scientists rank computational problems in three classes: easy, hard, and uncomputable (*1*). Recently, Adleman (*2*) showed that DNA can be used to solve a computationally hard problem, the Hamiltonian path problem, and demonstrated the potential power of parallel, high-density computation by molecules in solution. This parallelism allows DNA computers to solve larger hard problems such as NP-complete problems in linearly increasing time, in contrast to the exponentially increasing time required by a Turing machine. The trade-off is that DNA computers require exponentially increasing volumes of DNA. The ultimate success of DNA computing will be found in the details of algorithms taking advantage of massive parallelism. Despite valuable theoretical work (*3*, *4*), experiments of similar complexity to Adleman's have been few (*5*). Here, we present a molecular biology–based experimental solution to the maximal clique problem. We show (i) the solution to a problem in the same class (NP-complete) as the Hamiltonian path problem, (ii) a functional demonstration of improved design principles for DNA computing, and (iii) the use of living organisms (*Escherichia coli*) to read the answer of a computation.

Mathematically, a clique is defined as a set of vertices in which every vertex is connected to every other vertex by an edge. The maximal clique problem asks: Given a network containing $N$ vertices and M edges, how many vertices are in the largest clique? The graph of six vertices and 11 edges in Fig. 1a defines such a problem. The vertices (5,4,3,2) form the largest clique; thus, the size of the largest clique in this network is four. Finding the size of the largest clique has been proven to be an NP-complete problem (*6*). We designed the following algorithm to solve it:

1) For a graph with $N$ vertices, each possible clique is represented by an $N$-digit binary number. A bit set to 1 represents a vertex in the clique, and a bit set to 0 represents a vertex out of the clique. For example, the clique (4,1,0) is represented by the binary number 010011, whereas (5,4,3,2), the largest clique in Fig. 1a, is represented by the number 111100. In this way, we transform the complete set of possible cliques in an $N$-vertex graph into an ensemble of all $N$-digit binary numbers. We call this the complete data pool.

2) We find pairs of vertices in the graph that are not connected by an edge. The graph containing all edges missing in the

Q. Ouyang and P. D. Kaplan, NEC Research Institute, 4 Independence Way, Princeton, NJ 08540, USA.
S. Liu and A. Libchaber, NEC Research Institute, 4 Independence Way, Princeton, NJ 08540, USA, and Center for Studies in Physics and Biology, Rockefeller University, New York, NY 10021, USA.

*To whom correspondence should be addressed.

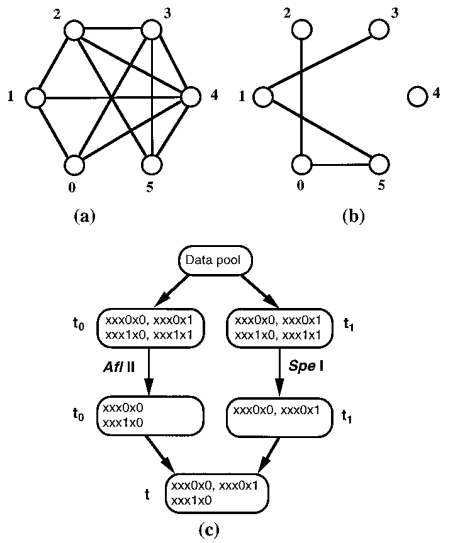


**Fig. 1.** The maximal clique problem. (**a**) The graph of our problem, in which the maximal clique is (5,4,3,2). (**b**) The complementary graph of (a), which gives connections between pairs of vertices that are absent in (a). (**c**) The logical process taken to remove numbers representing cliques connected by the 0-2 edge in (b).

**Fig. 2.** Encoding data in DNA. (**A**) The data structure of a six-digit number in DNA. (**B**) Assembling numbers by overlap extension. A full string of DNA in (A) is recursively assembled from short pieces by 3′ end hybridization and extension. The position and value string of DNA are denoted by bars and circles, respectively. The heavy arrows represent the ssDNA entering each stage of the reaction; the light lines represent extension.

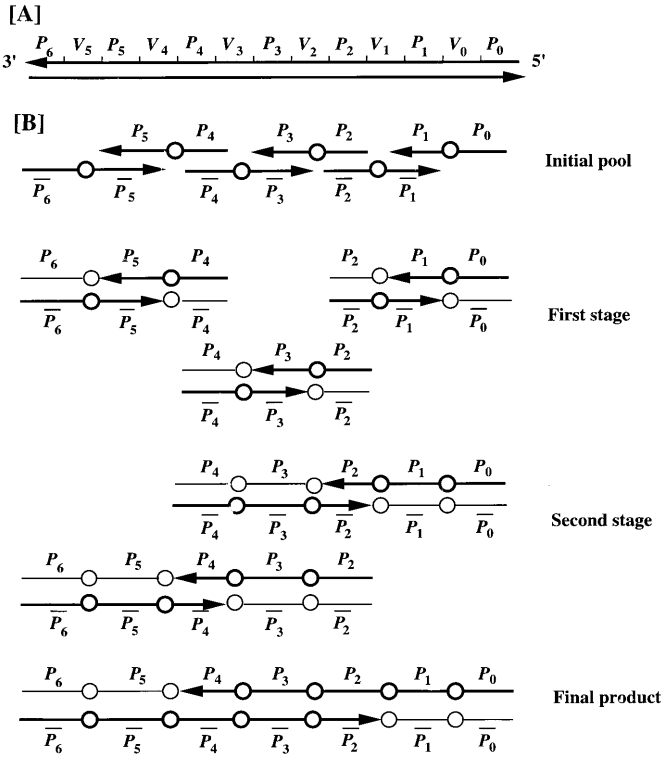


original graph is called the complementary graph (Fig. 1b). Any two vertices connected in the complementary graph are disconnected in the original graph (Fig. 1a) and therefore cannot be members of the same clique; this means that the corresponding bits cannot both be set to 1.

3) We eliminate from the complete data pool all numbers containing connections in the complementary graph. For our problem, the numbers xxx1x1, 1xxxx1, 1xxx1x, and xx1x1x are removed (x can be either 1 or 0). The remainder of the data pool corresponds to all cliques in the original graph.

4) We sort the remaining data pool to find the data containing the largest number of 1's. Each of these ones represents a vertex in the corresponding clique; therefore, the clique with the largest number of 1's tells us the size of the maximal clique.

The first task in DNA computing is to construct an ensemble of DNA molecules to represent the complete data pool. We designed the data structure in the form of double-stranded DNA (dsDNA). Each bit in a binary number is represented by two DNA sections corresponding to the bit's value ($V_i$) and its position ($P_i$). For a DNA molecule representing a six-digit binary number, there are six value sections ($V_0$ to $V_5$) sandwiched sequentially between seven position sections ($P_0$ to $P_6$) (Fig. 2A). The last position section, $P_6$, is needed for polymerase chain reaction (PCR) amplification. We found that $P_i$ with a length of 20 base pairs (bp) worked well (*7*). The length of $V_i$ was set to 0 bp if the value of $V_i = 1$, and to 10 bp if the value of $V_i = 0$. Therefore, the longest DNA has 200 bp corresponding to the number 000000, and the shortest DNA has 140 bp corresponding to the number 111111. This design is simple and effective, because we only need to know the number of 1's in the answer. The sequence of each $P_i$ and $V_i$ was first randomly generated. However, to avoid mispairing during data assembly, care was taken to avoid accidental homologies longer than 4 bp. For future convenience, we then embedded restriction sequences within each $V_i = 1$.

We used parallel overlap assembly (POA) (*7*) to construct our DNA data pool. This method (Fig. 2B) is broadly applied in gene construction (*8–10*), gene reconstruction (*11*), and DNA shuffling (*12*). The construction starts with the 12 oligonucleotides listed in Table 1. Each oligonucleotide consists of two position motifs and one value motif, $P_iV_iP_{i+1}$ for even $i$ and $\overline{P_{i+1}}V_i\overline{P_i}$ for odd $i$, where the bar represents the complementary sequence and the value of $V_i$ can be 0 or 1. The 12 fragment oligonucleotides were mixed together for thermal cycling (*13*). During each thermal cycle, the position strings in one oligonucleotide annealed to the complementary strings of the next oligonucleotide. The 3′ ends extended in the presence of polymerase to form a longer dsDNA. After a few thermal cycles, a data pool with all combinations of $V_0V_1V_2V_3V_4V_5$ was built (Fig. 2B). The POA procedure was followed by PCR with a small fraction of POA product serving as template and with $P_0$ and $\overline{P_6}$ acting as primers. Thus, only those molecules with $P_0$ and $P_6$ at their ends were exponentially amplified. The results of POA and PCR are shown in Fig. 3, lanes 2 and 3, respectively.

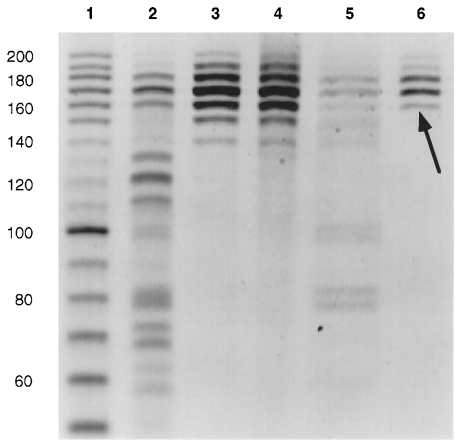


**Fig. 3.** Electrophoresis of products after each operation. Lane 1, marker; lane 2, product of POA; lane 3, product of PCR. The distribution of band intensities matches the expected binomial distribution. Lane 4, product of S1 nuclease digestion; lane 5, product of series restriction enzyme digestion; lane 6, product of final PCR (seven cycles). The band indicated by an arrow in lane 6 is the answer to the problem. The electrophoresis was conducted in 6% denatured polyacrylamide gel and stained by ethidium bromide.

Guided by the complementary graph (Fig. 1B), we digested the data pool with restriction enzymes (New England Biolabs). These enzymes break DNA at specific restriction sites, which we embedded within the sequences for $V_i = 1$. The broken strings were not amplified exponentially by PCR with primers $P_0$ and $\overline{P_6}$. To cut a connection in the complementary graph—for example, the 0-2 connection (Fig. 1c)—we first divided the data pool into two test tubes, $t_0$ and $t_1$. In $t_0$ we cut strings containing $V_0 = 1$ with Afl II; in $t_1$ we cut strings containing $V_2 = 1$ with Spe I. Next, we combined $t_0$ and $t_1$ into test tube $t$, which did not contain xxx1x1. Four sequential restriction operations (with different enzymes) eliminated all strings connected by edges in Fig. 1b, corresponding to data xxx1x1 (0-2 connection), 1xxxx1 (0-5 connection), 1xxx1x (1-5 connection), and xx1x1x (1-3 connection) (*14*). The remaining data DNA was then amplified by PCR. The results of restriction digestions and the PCR amplification are shown in Fig. 3, lanes 5 and 6, respectively.

Reading the size of the largest clique or cliques in the network is straightforward. In our data structure, the clique of largest size is represented by the shortest length of DNA, and thus the lowest band (arrow in Fig. 3, lane 6) is the answer. The length of this band, 160 bp, tells us that the size of the largest clique is four vertices.

Let us now push the problem a step further. Instead of asking for the size of the maximal clique, we ask: What is the maximal clique? Answering this question requires further processing because the molecules in Fig. 3, lane 6, could be any of 15 different DNA strings. We read the answer by molecular cloning. The DNA of the answer was first inserted into M13 bacteriophage (Phagescript, Stratagene) through site-specific mutagenesis (*15*). The mutagenized M13 phage DNA (containing our answer DNA) was transfected into *E. coli* bacteria (Xl-1 Blue, Stratagene), cloned, and its DNA extracted and sequenced (*16*). The result (Fig. 4) is the correct answer, 111100.

The major errors in this calculation come from two sources. The first source of error is the production of single-stranded DNA (ssDNA) during PCR. This ssDNA cannot be cut by restriction enzymes. We avoided this error by digesting the ssDNA with S1 nuclease (Promega) before restriction digestions (*17*) (Fig. 3, lane 4). This operation largely prevented false positive results.

The second source of error is incomplete cutting by restriction enzymes, which also leads to incorrect answers. The combination of restriction digestion and PCR forms an exponential amplifier with a larger exponent for uncut strands than for cut strands. Repeating the digestion-PCR process should therefore increase the signal-to-noise ratio arising from incomplete digestion. We used one and two cycles of digestion-PCR and found no qualitative difference. The selected restriction enzymes work well enough for our purpose.

Several comments are in order. Our algorithm tolerates point mutations because they do not significantly decrease the potential for annealing $P_i$ strands 20 nucleotides long. Point mutation within restriction sites is a more serious concern. However, given the rate of point mutation in PCR (known to be $10^{-4}$ per nucleotide per cycle for *Taq* polymerase) (*18*), there should be about three strands with mutations within restriction sites per 1000 copies of answer DNA. This error rate is comfortably buried in the background of electrophoresis gel images. The fidelity of PCR can be improved by using different polymerases. Point mutation is not the limitation to applying our algorithm to larger graphs.

The major advantage of DNA computing lies in its high parallelism. However, the number of vertices that this algorithm can handle is limited. The maximum number of vertices we can process with picomole operations is limited to 27 because of the exponential increase in the size of the pool with the size of the problem. With nanomole chemistry, we could have 36 vertices. Further scale-up quickly becomes impractical. New algorithms, resembling in vitro evolution in which the initial data pool need not contain every possible final answer, are needed.

As correctly stated by Adleman (*2*), the information storage capacity of DNA is huge. In principle, 1 μmol of DNA can encode 2 gigabytes of information. However, rapid and accurate data access is needed to take advantage of massive parallelism. Current techniques such as biotin-avidin purification (*2*), electrophoresis (*5*, *7*), and DNA cloning (as described above) are either too slow or too noisy. An automatic device, similar to the biochip developed recently by Affymetrix (*19*), is needed to accelerate readout.

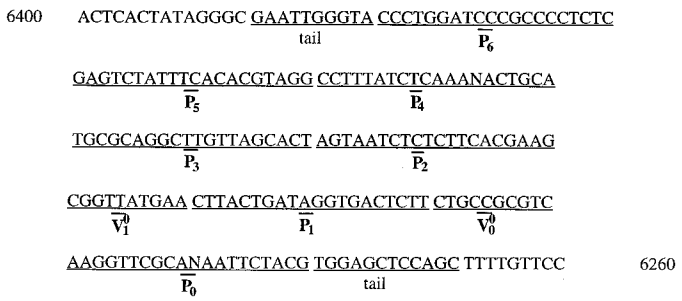


**Fig. 4.** The result of DNA cloning and sequencing. The inserted DNA is underlined and marked; the numbers indicate the locations of Phagescript M13 phage DNA. The letter N represents an undetermined base.

**Table 1.** Oligonucleotides used to construct the DNA data pool. Each string contains position sequences $P_i$ and value sequences $V_i^j$, where $j$ indicates the value of $V_i$. The value sequences are written with lowercase letters; restriction enzyme sites are indicated by underlining. Restriction enzymes Afl II, Hind III, Spe I, Sph I, Stu I, and Xho I (New England Biolabs) were applied to cut $V_0^1$, $V_1^1$, $V_2^1$, $V_3^1$, $V_4^1$, and $V_5^1$, respectively.

| DNA fragment | Sequence (5′ to 3′) |
|---|---|
| $P_0V_0^0P_1$ | CGTAGAATTCTGCGAACCTTgacgcggcagAAGAGTCACCTATCAGTAAG |
| $P_0V_0^1P_1$ | CGTAGAATTCTGCGAACCTTAAGAGTCACCTATCAGTAAG |
| $\overline{P_2V_1^0P_1}$ | AGTAATCTCTCTTCACGAAGcggttatgaaCTTACTGATAGGTGACTCTT |
| $\overline{P_2V_1^1P_1}$ | AGTAATCTCTCTTCACGAAGCTTACTGATAGGTGACTCTT |
| $P_2V_2^0P_3$ | CTTCGTGAAGAGAGATTACTccggtcacttAGTGCTAACAAGCCTGCGCA |
| $P_2V_2^1P_3$ | CTTCGTGAAGAGAGATTACTAGTGCTAACAAGCCTGCGCA |
| $\overline{P_4V_3^0P_3}$ | CCTTTATCTCAAAGACTGCAaatcgtcaggTGCGCAGGCTTGTTAGCACT |
| $\overline{P_4V_3^1P_3}$ | CCTTTATCTCAAAGACTGCATGCGCAGGCTTGTTAGCACT |
| $P_4V_4^0P_5$ | TGCAGTCTTTGAGATAAAGGaaaaacccacCCTACGTGTGAAATAGACTC |
| $P_4V_4^1P_5$ | TGCAGTCTTTGAGATAAAGGCCTACGTGTGAAATAGACTC |
| $\overline{P_6V_5^0P_5}$ | CCCTGGATCCCGCCCCTCTCagatcggtggGAGTCTATTTCACACGTAGG |
| $\overline{P_6V_5^1P_5}$ | CCCTGGATCCCGCCCCTCTCGAGTCTATTTCACACGTAGG |

## REFERENCES AND NOTES

1. For a general discussion, see J. Casti, *New Sci.* **2082**, 30 (1997).
2. L. M. Adleman, *Science* **266**, 1021 (1994).
3. R. J. Lipton, *ibid.* **268**, 542 (1995).
4. G. Paun, *J. Autom. Lang. Comb.* **1**, 27 (1996).
5. F. Guarnieri, M. Fliss, C. Bancroft, *Science* **273**, 220 (1996).
6. M. R. Garey and D. S. Johnson, *Computers and Intractability* (Freeman, New York, 1979).
7. P. D. Kaplan, Q. Ouyang, D. S. Thaler, A. Libchaber, *J. Theor. Biol.* **188**, 333 (1997), and references therein.
8. S. N. Ho, H. D. Hunt, R. M. Horton, J. K. Pullen, L. R. Pease, *Gene* **77**, 51 (1989).
9. K. Jayaraman, S. A. Fingar, J. Fyles, *Proc. Natl. Acad. Sci. U.S.A.* **88**, 4084 (1991).
10. W. P. Stemmer, A. Crameri, K. D. Ha, T. M. Brennan, H. L. Heyneker, *Gene* **164**, 49 (1995).
11. R. DeSalle, M. Barcia, C. Wray, *Experientia* **49**, 906 (1993).
12. W. P. Stemmer, *Proc. Natl. Acad. Sci. U.S.A.* **91**, 10747 (1994).
13. All PCR processes were performed on a Perkin-Elmer GeneAmp PCR system 9600 machine. For POA processing, 4 pmol of each DNA fragment and 2 units of AmpliTaq DNA polymerase, Stoffel fragment (Perkin-Elmer) in PCR buffer [10 mM tris-HCl, 50 mM KCl, 2.2 mM $MgCl_2$, 0.8 mM deoxynucleotide triphosphate (dNTP), pH 8.3, at 25°C] to a total volume of 40 μl were processed for 40 cycles (94°C for 30 s, 60°C for 30 s, and 72°C for 30 s). For general PCR, 0.2 μl of template solution, 20 pmol of primers, and 2 units of *Taq* DNA polymerase (Gibco-BRL) in PCR buffer [50 mM KCl, 10 mM tris-HCl, 2 mM $MgCl_2$, 10 mM $(NH_4)_2SO_4$, 0.8 mM dNTP, pH 8.8, at 25°C] to a volume of 40 μl were processed for 25 cycles (94°C for 30 s, 65°C for 30 s, and 72°C for 30 s).
14. The restriction enzyme digest operation was conducted following the protocol of New England Biolabs.
15. The mutagenesis process followed standard protocols (*20*): (i) We added a tail to the ends of answer DNA that is homologous (complementary) to parts of M13 phage DNA. PCR with specially designed primers was applied for this purpose. One primer consisted of 12-bp DNA homologous to M13 phage DNA (positions 6269 to 6280) and 15 bp of $P_0$ (GCTGGAGCTCCACGTAGAATTCTGCGA); the other primer consisted of 12-bp DNA complementary to M13 phage DNA (positions 6375 to 6386) and 15 bp of $\overline{P_6}$ (GAATTGGGTACCCTGGATCCCGCCC). The first primer was phosphorylated at the 5′ end with T4 polynucleotide kinase (New England Biolabs). (ii) The dsDNA of the PCR solution in step (i) was digested by λ exonuclease (Gibco-BRL) following the supplier's instructions. The DNA strand that contains a 5′ phosphate was thus digested. (iii) Mutagenetic M13 phage DNA (containing answer DNA) was synthesized using the ssDNA from step (ii) as primer and wild-type M13 phage DNA as template.
16. Transfection, phage purification, and DNA extraction were conducted following standard protocols (*20*). The DNA sequencing was done by the Rockefeller University Protein/DNA Technology Center.
17. The DNA in the data pool was purified by ethanol precipitation. The ssDNA was digested in S1 nuclease buffer (50 mM NaAc, 280 mM NaCl, and 4.5 mM $ZnSO_4$) with 2 units of S1 nuclease at room temperature for 2 min.
18. K. A. Eckert and T. A. Kunkel, *PCR Methods Appl.* **1**, 17 (1991).
19. M. Chee *et al.*, *Science* **274**, 610 (1996).
20. J. Sambrook, E. F. Fritsch, T. Maniatis, *Molecular Cloning* (Cold Spring Harbor Laboratory Press, Cold Spring Harbor, NY, 1987).


21. We thank D. Boneh, who proposed the maximal clique problem and the binary number–based algorithm for solving it, and D. Thaler, who suggested the use of POA to build the data pool.

23 June 1997; accepted 3 September 1997


# Direct Visualization of Individual Cylindrical and Spherical Supramolecular Dendrimers


S. D. Hudson,* H.-T. Jung, V. Percec,* W.-D. Cho, G. Johansson, G. Ungar,* V. S. K. Balagurusamy



Electron microscopy methods have been used to visualize individual spherical and cylindrical supramolecular dendrimers, providing definitive confirmation of the structures suggested by previous x-ray diffraction analysis that assumed a microsegregated model. These dendrimers are self-assembled, self-organized, and aligned spontaneously and simultaneously in hexagonal columnar or cubic thermotropic liquid-crystal phases with high uniformity. Homeotropic and planar ordering of the hexagonal columnar liquid crystal was precisely controlled by a variety of surfaces. The stiffness of these cylinders was evaluated by examining their planar texture and its defects.


Control of the order of molecular, macromolecular, and supramolecular synthetic organic materials is an important goal in chemistry, that can be used to improve the materials' properties (*1–3*). Building blocks based on dendritic architectures (*4*), which have a hierarchy of branched structures, can generate molecular objects of nanoscale dimensions (*5*, *6*), and self-assembly of supramolecular dendrimers from monodendritic building blocks can provide rapid access to the construction of giant architectures (*7*). The elucidation of the shape of dendrimers in solution and in the bulk represents one of the most important prerequisites for access to their controlled design (*4–6*). A transition from an ovoidal to a spherical shape by increasing the generation number has been predicted for dendrimers (*8*). Various studies have suggested that in solid and melt states, dendrimers or their aggregates, or both, can adopt either spherical (*5*) or rod-like shapes (*6*). However, because the previously studied dendritic systems lacked long-range positional order, individual objects could not be isolated, and therefore, the shape and size of these dendrimers could not be determined.

Recently, we have advanced a rational design and synthesized monodendrons that self-assemble through various molecular recognition mechanisms into rod-like (*9*), cylindrical (*10*), and spherical (*11*) supramolecular dendrimers. The cylindrical supramolecular dendrimers self-organize into a thermotropic hexagonal columnar ($\Phi_h$) (*10*) [two-dimensional (2D) p6mm lattice], whereas the spherical ones form a novel thermotropic cubic (Cub) liquid-crystalline (LC) phase of $Pm\bar{3}n$ symmetry (3D lattice) (*11*). The lattices of both supramolecular LC assemblies can be oriented by using techniques available for the alignment of molecular LC assemblies (*12*) to generate single-domain LCs. Analysis of mono- and polydomain LCs by x-ray diffraction (XRD) allowed the determination of the shape, size, and structure of supramolecular dendrimers organized in a lattice (*9–11*). However, owing to the ubiquitous phase problem, uncertainty is always present in crystallographic analyses based on limited numbers of reflections observed in LC systems (up to 13 different reflections obtained for **3**) (*11*). In our XRD experiments (*11*), the key assumption was that aromatic and aliphatic moieties segregate, aliphatic regions having uniform density. Thus, direct visualization of the structure by transmission electron microscopy (TEM) is invaluable in testing the assumptions on which the XRD structure is based (*13*). We directly imaged individual species of cylin-


S. D. Hudson, H.-T. Jung, V. Percec, W.-D. Cho, G. Johansson, The W. M. Keck Laboratories for Organic Synthesis, Department of Macromolecular Science, Case Western Reserve University, Cleveland, OH 44106–7202, USA.

G. Ungar and V. S. K. Balagurusamy, Department of Engineering Materials and Centre for Molecular Materials, The University of Sheffield, Sheffield S1 3JD, UK.

*To whom correspondence should be addressed.


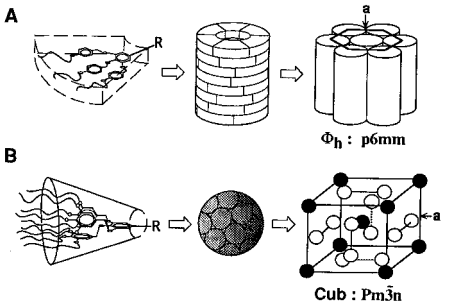


**Fig. 1.** Self-assembly of (**A**) first-generation flat tapered monodendrons into a supramolecular cylindrical dendrimer and the subsequent formation of the p6mm $\Phi_h$ LC supramolecular assembly, and (**B**) of second-generation conical monodendrons into a spherical dendrimer and the subsequent formation of the $Pm\bar{3}n$ Cub LC supramolecular assembly [modified version reprinted with permission from Balagurusamy *et al.* (*11*), copyright 1997 by American Chemical Society].